Journal of Materials Chemistry B

PAPER

View Article Online
View Journal

Cite this: DOI: 10.1039/c5tb01012h

TiO_2-B nanorod based competitive-like non-enzymatic photoelectrochemical sensing platform for noninvasive glucose detection†

Shupei Zhang,‡[a] Guifang Xu,‡[a] Lingshan Gong,[a] Hong Dai,*[a] Yilin Li,[a] Zhensheng Hong*[b] and Yanyu Lin[c]

Received 26th May 2015,
Accepted 25th August 2015

DOI: 10.1039/c5tb01012h

www.rsc.org/MaterialsB

TiO_2-B nanorods, with excellent properties including large specific surface area, open structures with significant voids, and continuous channels, were explored for the first time in the photoelectrochemical biosensing field. To reduce the destructive effect of UV light on biomolecules, dopamine was introduced onto the TiO_2-B nanorod surface through the coordination of dopamine to the undercoordinated titanium atoms of the TiO_2-B nanorods, which makes the complex a promising matrix for subsequent biosensing. Furthermore, concanavalin A as a recognition element was attached onto the TiO_2-B nanorod/dopamine modified electrode surface by virtue of covalent interaction between concanavalin A and dopamine. Accordingly, a new competitive-like non-enzymatic photoelectrochemical biosensor was established by using glucose labeled SiO_2 nanospheres of fixed concentration as photoelectrochemical signal inhibitors competing with target glucose of various concentrations for reaction with concanavalin A. Moreover, this ultrasensitive biosensor with excellent analytical performance was successful applied to noninvasive glucose determination in human saliva. Promisingly, the successful application of TiO_2-B nanorods in this research provides a new consideration in the selection of excellent photoactive materials for photoelectrochemical sensing.

1. Introduction

Photoelectrochemical (PEC) sensing, a newly emerged but dramatically progressing technique, is receiving increasing interest for sensing applications because of the easy operation and simplicity of the sensors.[1] Furthermore, some undesired background signals can be reduced greatly due to the efficient separation of the excitation source (light) and detection signals (photocurrent) in the PEC detection process, leading to high sensitivity and good analytical performance.[2] Undeniably, photoconversion efficiency plays a vital role in PEC detection sensitivity, which depends intimately on the photoactive materials immobilized on the substrate electrode.

From a materials perspective, TiO_2 is a promising candidate for PEC sensing due to its high photoactivity, nontoxicity, superior stability, earth-abundance and cost efficiency.[3,4] Among various polymorphs of TiO_2, TiO_2-B, a metastable phase of titania, owns a relatively more open structure with significant voids and continuous channels due to its perovskite-like layered structure and slightly lower density, which affords it a much higher charge–discharge capability and more excellent photoelectrical properties.[5,6] Therefore, TiO_2-B has drawn substantial attention in many fields including rechargeable lithium ion batteries, dye-sensitized solar cells, photocatalytic cells, sensors and supercapacitors.[7–11] However, to date, no successful attempt has been demonstrated using TiO_2-B as a scaffold for PEC sensing. Herein, TiO_2-B nanorods (TiO_2-B NRs) synthesized using a simple and additive-free strategy under solvothermal (acetic acid) conditions were used as photoactive species to explore their PEC performance in biosensing.

Many efforts have been focused on the exploration of TiO_2-based photocatalysts to decrease the mismatch of its optical band gap with the entire solar spectrum.[12,13] Interestingly, enediol ligands were found to have a large affinity for the undercoordinated surface Ti sites of TiO_2 species to form irreversible ligand-to-particle charge-transfer complexes, which endows the complex with a strong absorption ability in the visible light region.[14] Inspired by these, dopamine (DA) was introduced into this work. Herein, the localized orbitals of the surface attached DA ligands were electronically coupled with the delocalized electron levels of the conduction band (CB) of the

[a] College of Chemistry and Chemical Engineering, Fujian Normal University, Fuzhou, Fujian, 350108, China. E-mail: dhong@fjnu.edu.cn; Fax: +86-591-22866135
[b] Fujian Provincial Key Laboratory of Quantum Manipulation and New Energy Materials, College of Physics and Energy, Fujian Normal University, Fuzhou 350108, P. R. China. E-mail: winter0514@163.com
[c] Ministry of Education Key Laboratory of Analysis and Detection for Food Safety, and Department of Chemistry, Fuzhou University, Fuzhou 350002, P. R. China

† Electronic supplementary information (ESI) available. See DOI: 10.1039/c5tb01012h

‡ These authors equally contributed to this work.

TiO_2-B NRs, thus electrons can be excited under the illumination of visible light from the chelating ligands and then directly transfer into the CB of the TiO_2-B NRs.[15] In addition, complexes with outstanding PEC performance and good biocompatibility, can be used as a superior matrix to develop delicate PEC biosensors by using DA as a bridging linker.

Glucose, a small molecule, is the major energy source in the human metabolism process. Furthermore, the concentration of glucose in blood is considered as a crucial indicator in the diagnosis of diabetes, one of the leading diseases causing disability and death in humans. Accordingly, it is imperative to explore a reliable strategy for glucose detection, and many enzyme based biosensors have been fabricated because of their high selectivity and sensitivity.[16,17] To further expand the application scope, searching for enzyme-free sensors for glucose determination is of considerable interest.[18]

Herein, a sensitive non-enzymatic PEC biosensor was constructed based on a TiO_2-B NR/DA matrix for glucose detection by virtue of the high binding affinity between carbohydrates and concanavalin A (ConA). ConA, a lectin protein with four saccharide bind sites extracted from jack-beans, binds specifically to certain structures found in various sugars.[19,20] In addition, the amino group on lysine in ConA molecules affords a convenient site for immobilization onto other matrixes.[21] Therefore, ConA can be used as a bionic recognition device anchored onto the TiO_2-B NR/DA surface to specifically determine glucose concentration by recording the decreased photocurrent. To further amplify the variable value of the photocurrent, SiO_2 nanospheres (SiO_2 NSs), as signal-off labels, linked with glucose (SiO_2 NS–glucose) were used to compete with target glucose for specific recognition by ConA. Due to the large surface area, low toxicity, good stability and poor electroconductivity of SiO_2 NSs, SiO_2 NS–glucose can cause a greater decrease in the value of the photocurrent compared to glucose.[22,23]

2. Experimental

2.1 Materials and reagents

TiO_2 powder (P25) was obtained from Degussa Co. (Germany). Acetic acid (HAc), potassium hydroxide (KOH), ammonium hydroxide, *n*-hexanol, Triton X-100 (TX-100), acetone, ethanol, cyclohexane, tetraethyl orthosilicate (TEOS) and glucose were purchased from Sinopharm Chemical Reagent Co. (Shanghai, China). DA, glutaraldehyde (GLD, 25% aqueous solution), ConA and bovine serum albumin (BSA, 96–99%) were purchased from Aladdin Industrial Corporation (Shanghai, China), Shanghai Jinshan Tingxin Chemical Plant (China), Shanghai Yuanye Bio-Technology Co., Ltd (China) and Biss Inc. (Beijing, China), respectively. The phosphate buffer solution (PBS, 0.1 M, pH 7.4) as the supporting electrolyte was prepared by mixing a stock solution of 0.1 M NaH_2PO_4 and 0.1 M Na_2HPO_4 and adjusting the pH. Deionized water (DI water) used for the preparation of the solution was purified using a water purifier (China) purification system.

2.2 Apparatus

All of the PEC measurements were performed with a homemade PEC system under 395 nm irradiation. Photocurrents were recorded on a CHI 760 electrochemical workstation (Shanghai Chenhua Instrument Co., China) using a three-electrode system with a Ag/AgCl electrode (sat. KCl) as the reference electrode, platinum wire as the counter electrode and a modified glassy carbon electrode (3 mm in diameter) as the working electrode. Scanning electron microscopy (SEM, S4800 instrument) and transmission electron microscopy (TEM, FEI F20 S-TWIN instrument) were applied for the structural characterization of the products. X-ray diffraction (XRD) patterns were recorded on a PANalytical X'Pert spectrometer using Co Kα radiation (λ = 1.78897 Å), and the data were changed to Cu Kα data.

2.3 Synthesis of TiO_2-B NRs, SiO_2 NSs and SiO_2 NS–glucose conjugates

The TiO_2-B NRs were synthesized through a solvothermal (HAc) method using titanate nanowires as precursors. Synthesis of titanate nanowires is similar to our previous work.[24] Typically, 1 g of TiO_2 was dispersed in 75 mL of 15 M aqueous KOH solution. After stirring for 10 min, the resulting suspension was transferred into a 100 mL Teflon-lined stainless steel autoclave. The autoclave was kept at 170 °C for 72 h and then cooled to room temperature. The resulting precipitate was washed with diluted HAc solution until the pH was up to 7.0. The final product was then collected by centrifugation and dried at 60 °C for 12 h in air. The synthesis of TiO_2-B NRs was started by dispersing 300 mg of precursor titanate nanowires in 50 mL of 8 M HAc solution, and then transferred into a 100 mL Teflon-lined stainless steel autoclave, which was heated at 180 °C for 24 h. The final product was obtained by centrifuging and washing with distilled water and ethanol, and dried at 60 °C overnight.

SiO_2 NSs were synthesized using a revised method in a previous report.[25] Firstly, a mixed solution including 3.75 mL of cyclohexane, 885 μL of TX-100, 900 μL of *n*-hexanol and 170 μL of water was prepared. Then 30 μL of NH_4OH was added into the above mixture to initiate the polymerization reaction in the presence of 50 μL of TEOS. After the reaction was allowed to continue for 24 h under agitation, the product was isolated with acetone. Finally, the SiO_2 NSs were obtained by centrifugation and washed thoroughly with ethanol and water several times to remove any surfactant molecules, and dried at 60 °C overnight.

SiO_2 NS–glucose was prepared by mixing 500 μL of 1 mg mL^{-1} SiO_2 NSs and 500 μL of 10^{-5} mol L^{-1} glucose under sonication overnight at room temperature. Afterwards, the resulting mixture was centrifuged at 10 000 rpm for 30 min to obtain the precipitate, and then DI water was added to make a final volume of 1 mL for subsequent applications.

2.4 Fabrication of TiO_2-B NRs and TiO_2-B NR/DA modified electrodes

Prior to modification, the bare glassy carbon electrode (GCE) was polished with 0.3 and 0.05 μm alumina slurry on chamois

leather to produce a mirror-like surface, then it was washed successively with anhydrous alcohol and doubly distilled water in an ultrasonic bath and dried in air before use. With a micropipette, 4 μL of TiO_2-B NR solution was dropped onto the freshly prepared GCE surface and dried at room temperature, which was named TiO_2-B NRs.

Subsequently, with a micropipette, 10 μL of 0.015 M DA solution was dropped onto the TiO_2-B NR modified electrode, and then it was put in the dark for 20 min. Finally, the modified electrode was washed thoroughly with DI water to remove the DA of physical adsorption, and the modified electrode named TiO_2-B NR/DA.

2.5 Construction of the PEC biosensor

TiO_2-B NR/DA was subsequently immersed in 60 μL of GLD solution for 50 min to activate the NH_2 groups in DA and 60 μL of Con A (10^{-6} M) solution for 30 min to obtain TiO_2-B NR/DA/ConA. Afterwards, the modified electrode was immersed in 60 μL of BSA (1 wt%) for 1 h to block possible active sites. Finally, blocked TiO_2-B NR/DA/ConA was immersed in the mixture including a fixed concentration of SiO_2 NS–glucose and different concentrations of target glucose at 4 °C for 30 min. After each step, the electrode was washed thoroughly with DI water to remove the non-specific absorption.

2.6 Preparation of saliva samples

Saliva samples were collected from healthy volunteers (the experiment which involve the use of human subjects were performed in compliance with the relevant laws and institutional guidelines, and also state the institutional committees that have approved the experiments) after rinsing their mouths with water. Subsequently, the samples were centrifuged at 2000 rpm for 30 min to obtain the supernatants and then stored at −20 °C until analysis.

3. Results and discussion

3.1 Structure characterization of TiO_2-B NRs

To explore the morphology and microstructure of the TiO_2-B NRs, SEM, TEM and HRTEM images were investigated, as shown in Fig. 1. Obvious large-scale monodisperse rods can be seen in Fig. 1A. Besides, the nanorod structure, with nanorod lengths in the range of 45–60 nm, is further demonstrated in the low-resolution TEM image (Fig. 1B). The corresponding SAED pattern from an area of the nanorods presented the lattice planes of (020), (110) and (310) as shown in the inset of Fig. 1B, which is in good agreement with the monoclinic crystal structure of TiO_2-B. Furthermore, a well-crystallized structure with lattice fringes of about 0.62 nm is displayed in the HRTEM image (Fig. 1C), corresponding to the (001) plane of TiO_2-B. Remarkably, the width of the nanorods is tiny (around 7.5–8.5 nm), which is propitious to the fast transfer of electrons. Additionally, the phase structure and crystalline properties of the nanorods were further investigated and analysed using the XRD pattern in Fig. 1D. All of the diffraction peaks can be indexed as the monoclinic TiO_2-B phase (JCPDS 74-1940). The narrow sharp

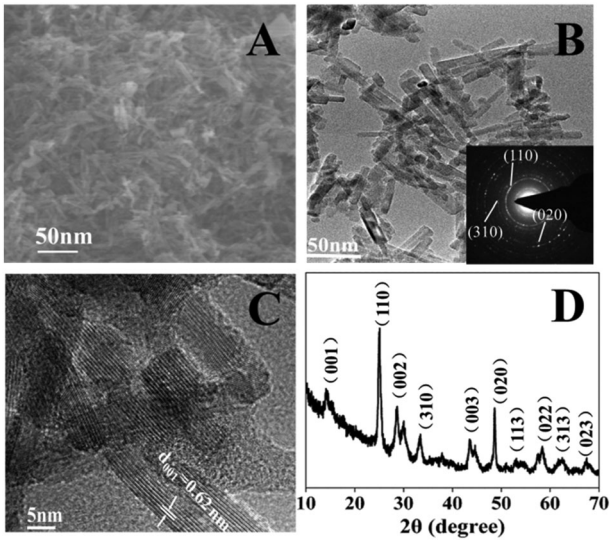

Fig. 1 (A) SEM image, (B) TEM image, (C) HRTEM image and (D) XRD pattern of the TiO_2-B NRs. The inset in (B) is a SAED pattern.

diffraction peaks at $2\theta = 14.2^\circ$, 25.1°, 28.6°, and 48.6° can be well assigned to the (001), (110), (002), and (020) lattice planes of TiO_2-B, respectively, implying that highly crystalline and only pure TiO_2-B formed in the products. The aforementioned findings clearly validate that the as-prepared material was a combination of nanorod morphology and a TiO_2-B polymorph.

Besides, N_2 adsorption–desorption isotherm measurements (data not displayed) revealed that the TiO_2-B nanorods have a large Brunauer–Emmett–Teller (BET) surface area (143 $m^2\ g^{-1}$) and high pore volume (0.73 $cm^3\ g^{-1}$), which are convenient for the selective incorporation of various guest materials, effective interfacial charge collection and the enhancement of light absorption.

3.2 Excellent PEC performance of TiO_2-B NR/DA

Although the significant voids and continuous channels of TiO_2-B NRs provide favourable conditions for PEC applications, the wide band gap of TiO_2-B limits its absorption in the visible region. Therefore, DA was introduced into this work in an attempt to enhance the PEC performance and photoelectric conversion efficiency. To certify the supposition, a series of PEC measurements were conducted. As depicted in Fig. 2A, compared with TiO_2-B NRs, TiO_2-B NR/DA exhibited a larger photocurrent density under all applied potentials, indicating that TiO_2-B NR/DA possessed a better PEC performance.

Fig. 2B displays the typical open-circuit photovoltage (V_{oc}) response under intermittent light illumination. The V_{oc} represents the difference in Fermi level between the photoactive materials (in this work these are the TiO_2-B NRs and TiO_2-B NR/DA) and counter electrodes. Under light illumination, most of the excited photoelectrons were collected within the TiO_2-B NRs or TiO_2-B NR/DA film, leading to a shift of the Fermi level to a more negative potential and the increase of the V_{oc}.[26,27] Therefore, the V_{oc} arrived at a steady state (maximum value) with the increase of photo-generated electrons in these thin-films under light illumination. Upon stopping the irradiation, the V_{oc} began to decay

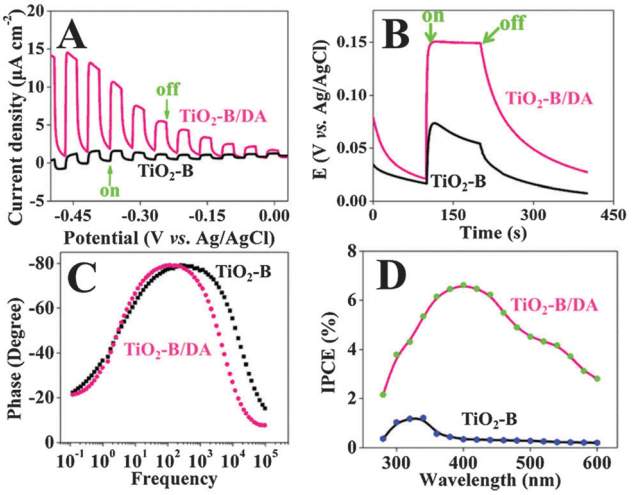

Fig. 2 (A) Photocurrent density–potential relationship under light on/off illumination, (B) open-circuit photovoltage responses, (C) Bode-phase plots of the TiO_2-B NRs and TiO_2-B NR/DA in 0.5 M Na_2SO_4, (D) IPCE spectra of the TiO_2-B NRs and TiO_2-B NR/DA in 0.1 M PBS (pH 7.0).

with the scavenging of the accumulated photoelectrons by the electron acceptor species in the solution and the recombination with photoholes. As expected, TiO_2-B NR/DA exhibited a higher photovoltage under light illumination and slower decay in the dark compared with the TiO_2-B NRs, suggesting a more efficient charge separation and less charge recombination for the TiO_2-B NR/DA complex, which was in good accordance with the results of the Bode-phase plots in Fig. 2C. The electron lifetime (τ_e) of the photoactive material was calculated according to the following eqn (1):[28]

$$\tau_e = \frac{1}{2\pi f_{max}} \quad (1)$$

where f_{max} is the frequency at which the peak appears in the plot. Clearly, the TiO_2-B NR/DA complex achieved a ms-scale lifetime (1.36 ms) which is about 23-fold slower than that of the pure TiO_2-B NRs (60 μs). Unquestionably, the slower recombination will result in more opportunities for electron–hole separation.

Furthermore, incident photon-to-electron conversation efficiency (IPCE) spectra were investigated to further elucidate the effect of DA, as shown in Fig. 2D. The IPCE values can be determined with no bias voltage based on eqn (2):[27]

$$IPCE\% = (1240 \times j \times 100)/(\lambda \times P) \quad (2)$$

where j is the measured photocurrent density in mA cm^{-2}, λ is the wavelength of the incident light in nm, and P is the power intensity of the incident light at each wavelength in mW cm^{-2}. Notably, the photoresponse of the pure TiO_2-B NRs in the visible light region was minimal until the irradiation wavelength blue-shifted to 380 nm, and then it sharply increased because the bandgap illumination was reached. Expectedly, the TiO_2-B NR/DA complex exhibited an enhanced photoresponse and higher IPCE value not only in the UV but also in the visible light region, which resulted from the large energy shift of the valence band in this complex.[14]

The aforementioned results are reasonable if taking into consideration the synergistic effect among the improved charge separation, elongated electron lifetime, and enhanced light absorption. The results strongly confirmed that the introduction of DA indeed dramatically improved the PEC performance of the TiO_2-B NRs. Accordingly, this complex with excellent photocatalytic performance is a promising candidate for PEC biosensing.

3.3 A tentative mechanism for the glucose detection

As a proof-of-concept application, a competitive-like enzyme-free PEC biosensor was developed as shown in Scheme 1A and a tentative mechanism for glucose determination is proposed in Scheme 1B. In this work, ConA was connected to the TiO_2-B NR/DA modified electrode surface using GLD as a bridging linker. Subsequently, glucose was anchored onto the electrode surface through the biospecific interactions between glucose and ConA, forming an immune complex-like moiety. Due to the inhibition of this immune complex-like moiety's ability to transfer O_2, the photocurrent decreased. To further amplify the change of photocurrent signal, SiO_2 NS–glucose competing with glucose was attached to ConA. The photocurrent density decreased with the decrease of glucose concentration because more and more SiO_2 NS–glucose anchored onto the modified electrode surface, which realized the ultrasensitive detection of glucose.

3.4 PEC biosensor characterization and detection strategy feasibility assay

To verify the above speculation, the stepwise fabrication process of this sensor was monitored as shown in Fig. 3A. In comparison with the GCE (a), the TiO_2-B NRs (b) presented a higher charge-transfer

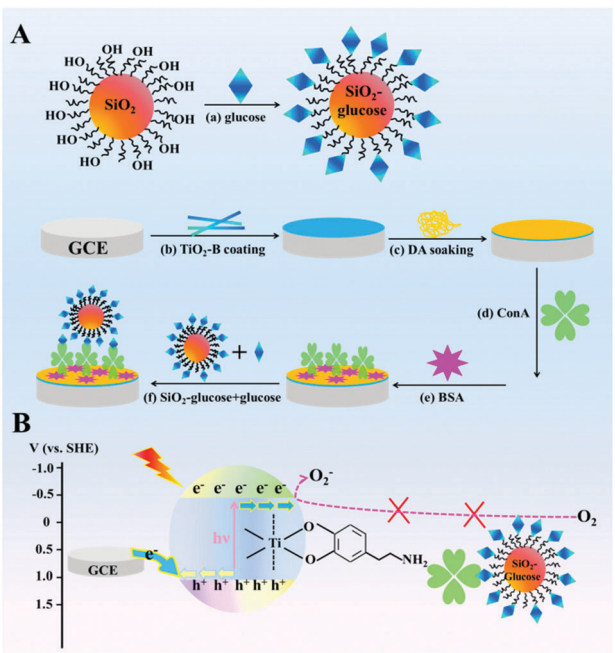

Scheme 1 (A) Schematic diagram of the competitive-like biosensor fabrication process. (B) Photocurrent generation mechanism of the PEC biosensor for glucose detection.

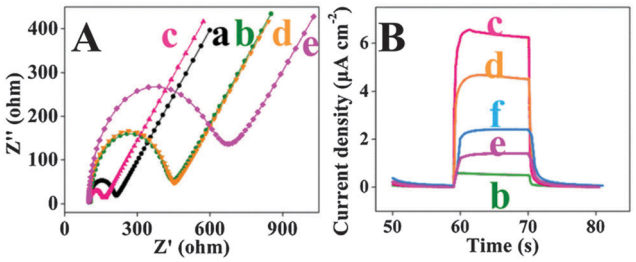

Fig. 3 (A) Nyquist diagrams of the EIS for different modified electrodes in 0.1 M KCl solution containing 5 mM $K_4[Fe(CN)_6]/K_3[Fe(CN)_6]$. (B) Photocurrent responses for different modified electrodes in 0.1 M PBS (pH 7.0) without a bias voltage: GCE (a), TiO_2-B NRs (b), TiO_2-B NR/DA (c), TiO_2-B NR/DA/ConA (d), TiO_2-B NR/DA/ConA incubation with a 20 μL mixture containing 10 μL of SiO_2 NS–glucose and 10 μL of 10^{-7} M (e) or 10^{-6} M (f) glucose.

resistance (R_{ct}) due to the poor electrical conductivity of the TiO_2-B NRs, implying that the TiO_2-B NRs were successful deposited onto the GCE. Obviously, the R_{ct} value reduced significantly after the successful formation of the DA–Ti complex (c) on the electrode surface, which could be explained as positively charged DA being in favor of the transfer of negatively charged $Fe(CN)_6^{3-/4-}$. As expected, the R_{ct} value gradually increased after TiO_2-B NRs/DA (c) was soaked in ConA (d), and the mixture of SiO_2 NS–glucose and glucose (e) solution, which resulted from the nonconductive properties of ConA and the SiO_2 NSs. The R_{ct} variation after each modification step provided solid evidence for the successful construction of this biosensor.

The photocurrent densities of different modified electrodes were investigated to probe the feasibility of this biosensor in Fig. 3B. As displayed in curve b, the TiO_2-B NRs demonstrated a sensitive PEC response because of their large specific surface area and more open structure, which was propitious to the effective interfacial charge capture, enhanced light-scattering ability, and fast electrolyte diffusion. Expectedly, TiO_2-B NRs/DA (c) exhibited a profound increased cathode photocurrent response (which can be proved in Fig. S2, ESI†) induced by the photoelectrons moving from the chelating DA directly into the CB of the TiO_2-B NRs. Subsequently, after the successful assembly of ConA (d) and SiO_2 NS–glucose (e and f), the photocurrent density gradually decreased due to the steric hindrance of ConA and the SiO_2 NSs. As exhibited in curve e and f, the photocurrent increased with the increase of glucose concentration. Based on the above investigation, we believe that the designed sensing strategy could be applied to detect glucose.

3.5 Analytical performance of the biosensor

Under the optimum conditions (Fig. S3 and S4, ESI†), the photocurrent densities of TiO_2-B NR/DA/ConA after incubation in mixtures of a fixed SiO_2 NS–glucose concentration and various glucose concentrations were recorded to evaluate the detection performance of this biosensor. As manifested in Fig. 4A, the photocurrent densities increased with the increase of target glucose concentration. In addition, the variation values of photocurrent density linearly increased with an increasing logarithm of glucose concentration in the range of 5×10^{-8} M to 10^{-3} M with a detection limit of 1.7×10^{-8} M (Fig. 4B), which exceeded previous reports (Table S1, ESI†).

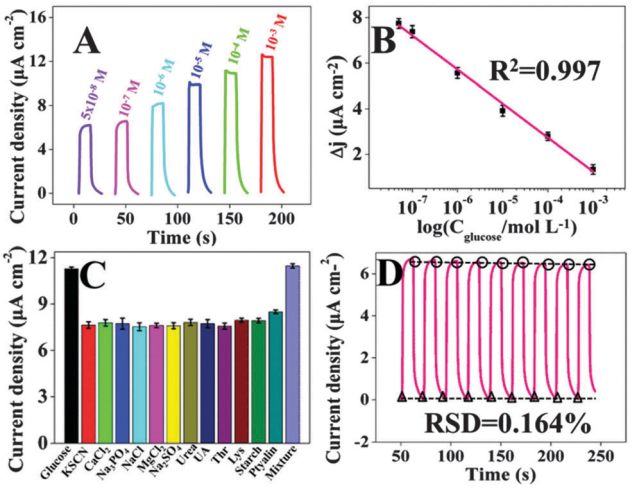

Fig. 4 (A) The photocurrent densities for the detection of different concentrations of target glucose. (B) The corresponding calibration curve. (C) The photocurrent densities of the prepared sensor to glucose with interfering substances. (D) The photocurrent response of the biosensor with 10^{-7} M target glucose under repeat on/off cycles of simulated light. 0.1 M PBS (pH 6.0), −0.2 V.

To explore the specificity of this sensor, some potential interfering substances at an excess of 20 fold the concentration of the glucose concentration were examined in Fig. 4C. Significantly, a negligible change of photocurrent density was displayed, which clearly confirmed that this strategy possessed a reasonable selectivity towards glucose detection.

Furthermore, the stability and reproducibility of this biosensor are crucial for practical applications. As provided in Fig. 4D, not only a strong and stable photocurrent was observed under light illumination but also the positions of the dark current (zero) did not change, implying an excellent chemical and structural stability. Besides, there was no obvious photocurrent deterioration after 15 days storage at 4 °C, which indicated that the biosensor possesses good storage stability.

Additionally, reproducibility as an important criterion was investigated by testing five freshly fabricated modified electrodes. Under the same conditions, the results manifested an almost identical photocurrent with a RSD of 4.72%, predicting that the biosensor has good fabrication reproducibility.

To examine the applicability, the proposed competitive-like non-enzymatic biosensor was used to detect glucose in human saliva (the concentration of glucose in saliva is *ca.* 1% of that in blood). The results (Table S2, ESI†) displayed that the glucose concentration in the five healthy humans was lower than 80 μM, which was in good accordance with the results in previous reports.[29,30] In addition, the recovery of these five saliva samples was in the range of 96.1% to 104.6%, demonstrating that the designed biosensor can be used in clinical applications for ultrasensitive glucose determination in human saliva.

4. Conclusions

In summary, DA sensitized TiO_2-B NRs with outstanding PEC performance in the visible light region and SiO_2 NSs with poor

electroconductivity as a matrix and as signal-off labels, respectively, were used for ultrasensitive glucose detection by means of the biospecific interaction between ConA and glucose. This biosensor displayed excellent analytical performance including a wide linear range, high sensitivity, good specificity and robust stability. Especially, the wide linear range covered the glucose concentrations not only in blood but also in saliva. Therefore, the biosensor provided convenient conditions for noninvasive glucose detection in human saliva, which eliminates pain, discomfort and superinfection originating from a punctured finger. Furthermore, the dissolved oxygen in the solution had a positive effect on the cathode photocurrent during the PEC biosensing, which avoided the addition of supplementary substrates and the destructive effects of photo-generated holes to biomolecules. Unquestionably, this research not only depicts a successful paradigm for the exploration of the fascinating properties of TiO_2-B NRs in a new application field, but also paves a new path for developing high performance PEC biosensors.

Acknowledgements

This project was financially supported by the NSFC (21205016, 21575024), National Science Foundation of Fujian Province (2011J05020), and Education Department of Fujian Province (JA14071, JB13008, JA13068). The Fujian Normal University outstanding young teacher research fund project (fjsdjk2012068) is also greatly acknowledged.

Notes and references

1 Y. T. Long, C. Kong, D. W. Li, Y. Li, S. Chowdhury and H. Tian, *Small*, 2011, **7**, 1624.
2 H. B. Li, J. Li, Q. Xu and X. Y. Hu, *Anal. Chem.*, 2011, **83**, 9681.
3 X. B. Chen, S. H. Shen, L. J. Guo and S. S. Mao, *Chem. Rev.*, 2010, **110**, 6503.
4 P. Hartmann, D. K. Lee, B. M. Smarsly and J. Janek, *ACS Nano*, 2010, **4**, 3147.
5 A. G. Dylla, G. Henkelman and K. J. Stevenson, *Acc. Chem. Res.*, 2013, **46**, 1104.
6 T. Kogure, T. Umezawa, Y. Kotani, A. Matsuda, M. Tatsumisago and T. Minami, *J. Am. Ceram. Soc.*, 1999, **82**, 3248.
7 A. R. Armstrong, G. Armstrong, J. Canales, R. Garcia and P. G. Bruce, *Adv. Mater.*, 2005, **17**, 862.
8 K. Asagoe, S. Ngamsinlapasathian, Y. Suzuki and S. Yoshikawa, *Cent. Eur. J. Chem.*, 2007, **5**, 605.
9 C. H. Lin, J. H. Chao, C. H. Liu, J. C. Chang and F. C. Wang, *Langmuir*, 2008, **24**, 9907.
10 G. Wang, Q. Wang, W. Lu and J. H. Li, *J. Phys. Chem. B*, 2006, **110**, 22029.
11 Q. Wang, Z. H. Wen and J. H. Li, *Adv. Funct. Mater.*, 2006, **16**, 2141.
12 P. Roy, C. Das, K. Lee, R. Hahn, T. Ruff, M. Moll and P. Schmuki, *J. Am. Chem. Soc.*, 2011, **133**, 5629.
13 X. Chen, L. Liu, P. Y. Yu and S. S. Mao, *Science*, 2011, **331**, 746.
14 T. Rajh, L. X. Chen, K. Lukas, T. Liu, M. C. Thurnauer and D. M. Tiede, *J. Phys. Chem. B*, 2002, **106**, 10543.
15 N. M. Dimitrijevic, Z. V. Saponjic, B. M. Rabatic and T. Rajh, *J. Am. Chem. Soc.*, 2005, **127**, 1344.
16 J. Wang, *Chem. Rev.*, 2008, **108**, 814.
17 C. Chen, Q. J. Xie, D. W. Yang, H. L. Xiao, Y. C. Fu, Y. M. Tan and S. Z. Yao, *RSC Adv.*, 2013, **3**, 4473.
18 T. W. Tsai, G. Heckert, L. F. Neves, Y. Tan, D. Y. Kao, R. G. Harrison, D. E. Resasco and D. W. Schmidtke, *Anal. Chem.*, 2009, **81**, 7917.
19 D. P. Tang, B. Zhang, J. Tang, H. Li and G. N. Chen, *Anal. Chem.*, 2013, **85**, 6958.
20 Z. H. Chen, Y. Liu, Y. Z. Wang, X. Zhao and J. H. Li, *Anal. Chem.*, 2013, **85**, 4431.
21 S. Q. Liu, K. W. Wang, D. Du, Y. M. Sun and L. He, *Biomacromolecules*, 2007, **8**, 2142.
22 M. Liong, J. Lu, M. Kovochich, T. Xia, S. G. Ruehm, A. E. Nel, F. Tamanoi and J. I. Zink, *ACS Nano*, 2008, **2**, 889.
23 J. Kim, H. S. Kim, N. Lee, T. Kim, H. Kim, T. Yu, I. C. Song, W. K. Moon and T. Hyeon, *Angew. Chem.*, 2008, **120**, 8566.
24 H. Dai, S. P. Zhang, L. S. Gong, Y. L. Li, G. F. Xu, Y. Y. Lin and Z. S. Hong, *Biosens. Bioelectron.*, 2015, **72**, 18.
25 S. Santra, P. Zhang, K. Wang, R. Tapec and W. H. Tan, *Anal. Chem.*, 2001, **73**, 4988.
26 B. H. Meekins and P. V. Kamat, *ACS Nano*, 2009, **3**, 3437.
27 X. M. Song, J. M. Wu, M. Z. Tang, B. Qi and M. Yan, *J. Phys. Chem. C*, 2008, **112**, 19484.
28 F. L. Gou, X. Jiang, B. Li, H. W. Jing and Z. P. Zhu, *ACS Appl. Mater. Interfaces*, 2013, **5**, 12631.
29 F. A. Wang, X. Q. Liu, C. H. Lu and I. Willner, *ACS Nano*, 2013, **7**, 7278.
30 D. X. Ye, G. H. Liang, H. X. Li, J. Luo, S. Zhang, H. Chen and J. L. Kong, *Talanta*, 2013, **116**, 223.

